Spontaneously Formed Unilamellar Vesicles with Path-Dependent Size Distribution

Mu-Ping Nieh,[†] Velayudhan A. Raghunathan,[†,‡] Steve R. Kline,[§] Thad A. Harroun,[†,||] Chien-Yueh Huang,[⊥] Jeremy Pencer,[†,#] and John Katsaras*[,†]

National Research Council, Steacie Institute for Molecular Sciences, Chalk River, Ontario K0J 1J0, Canada, Raman Research Institute, Bangalore 560 080, India, National Institute of Standards and Technology, Gaithersburg, Maryland 20899, Department of Physics, University of Guelph, Guelph, Ontario N1G 2W1, Canada, York Department of Chemical Engineering, New Jersey Institute of Technology, Newark, New Jersey 07102, and Department of Physics, St. Francis Xavier University, Antigonish, Nova Scotia B2G 2W5, Canada

Received April 5, 2005. In Final Form: May 25, 2005

We observe the spontaneous formation of path-dependent monodisperse and polydisperse phospholipid unilamellar vesicles (ULV) from two different equilibrium morphologies specifically, disklike micelles and extended lamellae, respectively. On heating beyond a temperature T_c, low temperature disklike micelles, or so-called bicelles, transform into lamellae. Dilution of the lamellar phase, at a fixed temperature, results in a complete unbinding transition and the formation of polydisperse ULV, demonstrating the instability of the lamellar phase. On the other hand, heating of a dilute bicellar phase above T_c results in monodisperse ULV, which on cooling revert back to bicelles for lipid concentrations $\phi \geq 0.5$ wt % and transform into oblate ellipsoids for $\phi = 0.1$ wt %, a morphology not previously seen in "bicellar" lipid mixtures. Monodisperse ULV reform on heating of the oblate ellipsoids.

1. Introduction

The repeat spacing d of a stack of L_α bilayers, or lamellae, is determined by the balance between the attractive and repulsive interbilayer interactions.[1,2] In the case of some ionic amphiphiles, electrostatic repulsion dominates over van der Waals attraction, at all bilayer separations. In this case, d is determined by the amount of water present in the sample and continuously increases as the sample is diluted. At a critical dilution, the lamellar stack breaks up into a dispersion of entropically favored, uncorrelated bilayers. This transformation is commonly referred-to as a complete unbinding transition.[3] Due to their high edge energy, the unbound bilayer fragments generally "close" to form almost spherical unilamellar vesicles (ULV), as shown in Figure 1a. Since there is no preferred size for these fragments, the resultant ULV are highly polydisperse.[4]

In amphiphile−water systems, ULV are also known to spontaneously form under a different set of conditions.[5] For example, in binary mixtures consisting of oppositely charged surfactants, ULV are found within a certain range of compositions.[6] Their size is usually well defined, and they are believed to be energetically stabilized. Different mechanisms have been proposed for their formation, including a negative modulus of Gaussian curvature resulting from charged bilayers,[7] and a nonzero spontaneous curvature arising from the unequal distribution of the two molecular species making up the inner and outer leaflets of the bilayer.[8,9] In other binary systems, such as

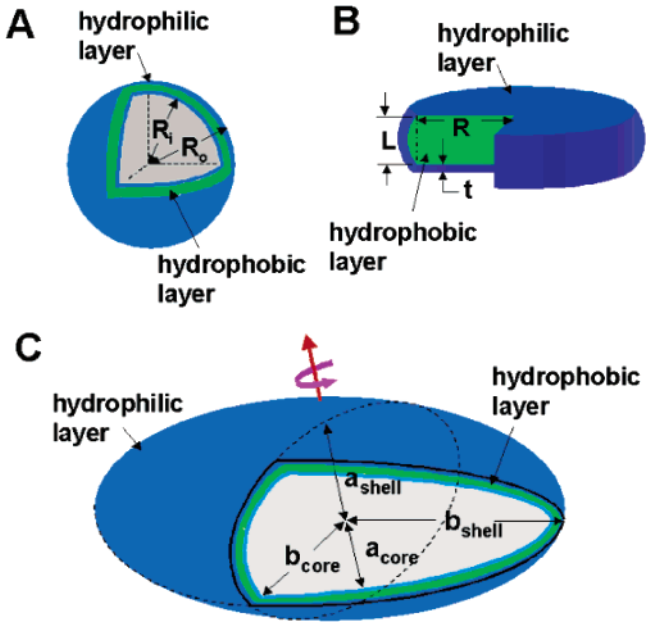

Figure 1. Various morphologies assumed by the lipid mixtures studied. (a) ULV made up of a single lipid bilayer containing and surrounded with aqueous solution. The hydrophilic headgroups are dissolved in solution while the hydrophobic hydrocarbon chains are sequestered. R_i and R_o are the inner and outer radii, respectively. $R_o - R_i = \delta$. (b) Bilayered micelle or commonly referred to bicelle. R ~ the radius of the bicelle, while L and t correspond to the thickness of the hydrophobic and hydrophilic layers, respectively. c) Oblate ellipsoid. a_{shell}, b_{shell}, a_{core}, and b_{core} correspond to the various minor and major axes radii of the oblate ellipsoid's shell and core, respectively.

* To whom correspondence should be addressed.
† Steacie Institute for Molecular Sciences.
‡ Raman Research Institute.
§ National Institute of Standards and Technology.
|| University of Guelph.
⊥ New Jersey Institute of Technology.
St. Francis Xavier University.

(1) Isrealachvilli, J. *Intermolecular and Surface Forces*, 2nd ed.; Academic Press: New York, 2000.
(2) Gelbart, W. M., Ben-Shaul, A., Roux, D., Eds.; *Micelles, Membranes, Monolayers, and Microemulsions*; Springer: New York, 1994.
(3) Leibler, S.; Lipowsky, R. *Phys. Rev. B* **1987**, *35*, 7004−7009.
(4) Demé, B.; Dubois, M.; Gulik-Krzywicki, T.; Zemb, T. *Langmuir* **2002**, *18*, 997−1004.
(5) Gradzielski, M. *J. Phys.: Condens. Matter* **2003**, *15*, R655−R697.
(6) Kaler, E.; Murthy, A. K.; Rodriguez, B. E.; Zasadzinski, J. A. N. *Science* **1989**, *245*, 1371.
(7) Winterhalter, M.; Helfrich, W. *J. Phys. Chem.* **1992**, *96*, 327−330.

10.1021/la0508994 CCC: $30.25
Published on Web 06/17/2005

mixtures of lecithin and bile salt, monodisperse ULV are known to form as a result of a specific temporal evolution of the amphiphile aggregate morphology following dilution.[10] In the case of disklike micelles, their edge energy (Figure 1b) makes them unstable above a critical size resulting in the formation of ULV.[11,12] The critical disk radius is determined by the balance between the edge energy of the bicelle and the curvature energy of the ULV and is given by $R_d = (2\kappa + \bar{\kappa})/\gamma$, where κ and $\bar{\kappa}$ are the bending and Gaussian moduli of the bilayer, respectively, and γ is the disk line tension.

Among the variety of spontaneously forming ULV systems, it is asserted that those formed by phospholipids are not equilibrium structures but are kinetically trapped.[12,13] However, determining whether ULV are thermodynamically stable or kinetically trapped is nontrivial. The observation of reversible ULV formation induced by a change in temperature has been suggested as one criterion of thermodynamic stability.[13,14]

Recently, we have reported the formation of reasonably monodisperse ULV in a ternary phospholipid mixture consisting of the zwitterionic lipids dimyristoyl phosphatidylcholine (DMPC) and dihexanoyl phosphatidylcholine (DHPC) and the anionic lipid dimyristoyl phosphatidylglycerol (DMPG).[15,16] The system's phase diagram is dominated by three liquid crystalline morphologies. Below a critical temperature T_c, comparable to the chain melting transition temperature ($T_M \simeq 23$ °C) of DMPC, the mixture exhibits an isotropic dispersion of disklike micelles over a wide range of total lipid concentration (ϕ). At temperatures above T_c, a lamellar phase is found for $\phi \gtrsim 2$ wt %,[17−19] whereas at lower concentrations, monodisperse ULV are obtained.

The purpose of these earlier studies was to determine the morphologies of the so-called "bicellar" system using an independent method from the more commonly favored nuclear magnetic resonance (NMR) technique. However, the results raised several questions regarding the thermodynamics of the system. First, do lamellae undergo a complete unbinding transition at 2 wt % as the data seem to indicate? Since the samples were previously diluted only at low T, and the lamellar and ULV phases were formed independently by raising the temperature from the bicelle phase, would the ULV form from lamellae if the sample were diluted at higher T? Second, what dictates the size of ULV, if anything? This system may be highly suited for studying the thermodynamic stability of ULV, since this morphology may be formed either by the dilution of L_α bilayers or by heating a dilute isotropic micellar solution. Finally, are the various transitions reversible? The occurrence of an isotropic phase may erase any memory of previous phases.

To answer these questions, we devised a series of small angle neutron scattering (SANS) experiments whereby we explored the formation of the various morphologies from different paths in order to gain better insight as to how these disparate morphologies form. The strategy was to take samples through dilution at high and low T, and then cycle the temperature as appropriate. From these studies, we have made three key observations. First, the lamellar phase undergoes an unbinding transition to ULV at $\phi \sim 2$ wt %. The fact that the boundary between ULV and lamellar phases occurs at the same ϕ, regadless of formation path, stongly indicates they are the thermodynamically stable phases above T_c. Second, the size of ULV are stongly dependent on both ϕ and sample history. This is discussed in detail in conjunction with the last point, in which some ULV do not revert to bicelles with decreasing temperature and instead form oblate ellipsoids shells with the same lipid mass. This provides evidence that the ULV are *both* an equilibrium morpholgy and kinetically trapped in size.

2. Materials and Methods

Dimyristoyl phosphatidylcholine (DMPC), dihexanoyl phosphatidylcholine (DHPC), and dimyristoyl phosphatidylglycerol (DMPG) were purchased from Avanti Polar Lipids (Alabaster, AL) and used without further purification. [The identification of any commercial product or trade name does not imply endorsement or recommendation by the National Institute of Standards and Technology.] Samples are prepared as follows: A 25 wt % lipid mixture is first dispersed in D_2O (99.9% in purity, Chalk River Laboratories) using the same preparation procedure reported by Nieh et al.[18,19] Samples (18 to 0.1 wt %) are then prepared by diluting the 25 wt % mixture at 45 °C with D_2O. Each sample is then vortexed for a minimum of 1 min at 45 °C. Samples were then transferred to the sample chamber, which was preheated to 45 °C, and their SANS profiles were recorded (Figure 2). Data were again collected after cooling to 10 °C and on subsequent reheating to 45 °C (Figure 3). Another set of samples (2.5−0.1 wt %) is also made from the same 25 wt % mixture by diluting at 4 °C. For lipid concentrations $\phi \geq 5$ wt %, samples were loaded into quartz sample cells with a gap of 1 mm. For $\phi \leq 2.5$ wt % a 2 mm cell was used. Each measurement was taken after the sample was equilibrated at the desired temperature for about 30 min. For all samples, the molar ratios of ([DMPC]+[DMPG])/[DHPC] and [DMPG]/[DMPC] were fixed at 3.2 and 0.01, respectively.

Experiments are performed using the 30-m SANS instrument (NG7) located at the National Institute of Standards and Technology (Gaithersburg, MD). The neutron wavelength λ is 8.09 Å, and three sample-to-detector distances (1.0, 5.0 and 15.3 m) are used to cover a range of the magnitude of the scattering vector, q ($= 4\pi \sin(\theta/2)/\lambda$, where θ is the scattering angle), from 0.002 to 0.35 Å^{-1}. Data, collected on a 2-dimensional detector, are then corrected for background and reduced to an absolute intensity scale. The data are subsequently circularly averaged to obtain the scattered intensity $I(q)$.

SANS data for the various morphologies are fitted with models described in the Appendix, incorporating the instrumental resolution. Although the models used have some limitations, nevertheless the χ^2 values for all fits ranged from 0.04 (bicelles, Figure 3) to 0.02 (oblate ellipsoid, Figure 5). This indicates the high degree of confidence that the appropriate model was used to fit the data.

3. Results and Discussion

High-T Dilution. The first experiment involves diluting the 25 wt % sample in single steps, at 45 °C, to final concentrations of 18.0, 12.5, 9.0, 5.0, 2.5, 1.25, 0.5, and 0.1 wt %. All of the inital data following dilution are shown in Figure 2. Samples with $\phi \geq 2.5$ wt % exhibit Bragg

(8) Safran, S. A.; Pincus, P.; Andelman, D. *Science* **1990**, *248*, 354−356.
(9) Safran, S. A.; Pincus, P.; Andelman, D.; MacKintosh, F. C. *Phys. Rev. A* **1991**, *43*, 1071.
(10) Egelhaaf, S. U.; Shurtenberger, P. *Phys. Rev. Lett.* **1999**, *82*, 2804−2807.
(11) Fromherz, P. *Chem. Phys. Lett.* **1983**, *94*, 259−266.
(12) Leng, J.; Egelhaaf, S. U.; Cates, M. E. *Biophys. J.* **2003**, *85*, 1624−1646.
(13) Marques, E. F. *Langmuir* **2000**, *16*, 4798−4807.
(14) Cantù, L.; Corti, M.; Musolino, M.; Salina, P. *Europhys. Lett.* **1990**, *13*, 561.
(15) Nieh, M.-P.; Harroun, T.; Raghunathan, V. A.; Glinka, C. J.; Katsaras, *J. Phys. Rev. Lett.* **2003**, *91*, 158105.
(16) Nieh, M.-P.; Harroun, T. A.; Raghunathan, V. A.; Glinka, C. J.; Katsaras, J. *Biophys. J.* **2004**, *86*, 2615.
(17) Katsaras, J.; Donaberger, R. L.; Swainson, I. P.; Tennant, D. C.; Tun, Z.; Vold, R. R.; Prosser, R. S. *Phys. Rev. Lett.* **1997**, *78*, 899.
(18) Nieh, M.-P.; Glinka, C. J.; Krueger, S.; Prosser, R. S.; Katsaras, J. *Langmuir* **2001**, *17*, 2629−2638.
(19) Nieh, M.-P.; Glinka, C. J.; Krueger, S.; Prosser, R. S.; Katsaras, J. *Biophys. J.* **2002**, *82*, 2487−2498.

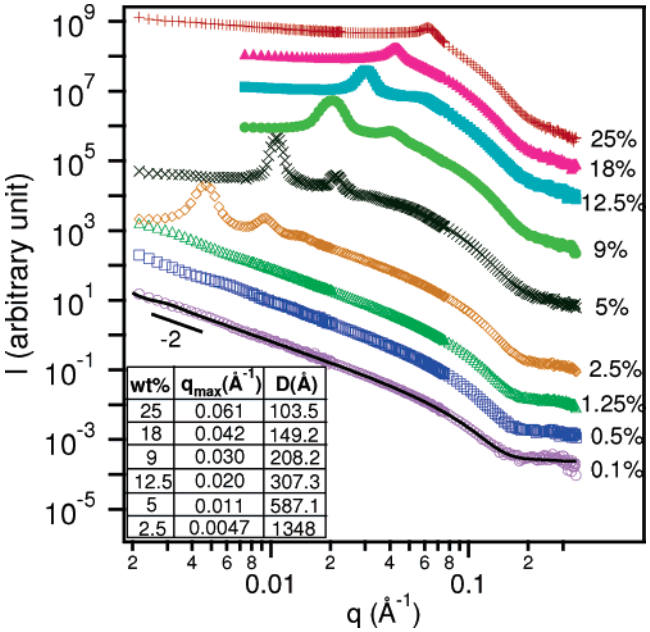

Figure 2. SANS profiles of samples diluted at 45 °C. The profiles for $\phi \geq 2.5$ wt % are characteristic of equidistant lamellae. The scattered intensity for $\phi \leq 1.25$ wt % follows a q^{-2} dependence, indicative of isolated bilayers. The solid line is a fit to the data from the 0.1 wt % sample using a model of noninteracting polydisperse ULV (see text). The number and "sharpness" of the various lamellar peaks, as a function of ϕ, are due to a combination of the number of correlated bilayers (i.e., width of peak) and the number of bilayers contributing to the scattering (i.e., signal-to-noise).

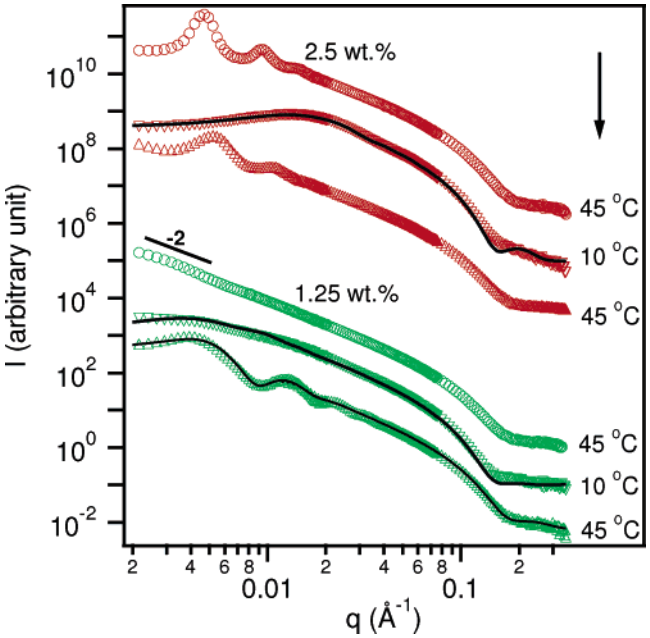

Figure 3. SANS profiles of 2.5 and 1.25 wt % samples prepared at 45 °C (top) on cooling to 10 °C (middle) and on reheating to 45 °C (bottom). The arrow represents the sequence used for temperature cycling. The lamellar phase is recovered in the 2.5 wt % sample, whereas for the 1.25 wt % sample, initially polydisperse ULV become monodisperse on reheating. The solid lines are fits to the data from the 1.25 wt % sample at 10 and 45 °C using models of bicelles and ULV in combination with the S_HP structure factor, respectively (see the Appendix).

maxima, typical of a lamellar phase. The lamellar repeat distance d varies linearly with changes in ϕ^{-1}, from 104 to 1348 Å with decreasing concentration. There is indirect evidence that the lamellae contain pore-like curvature

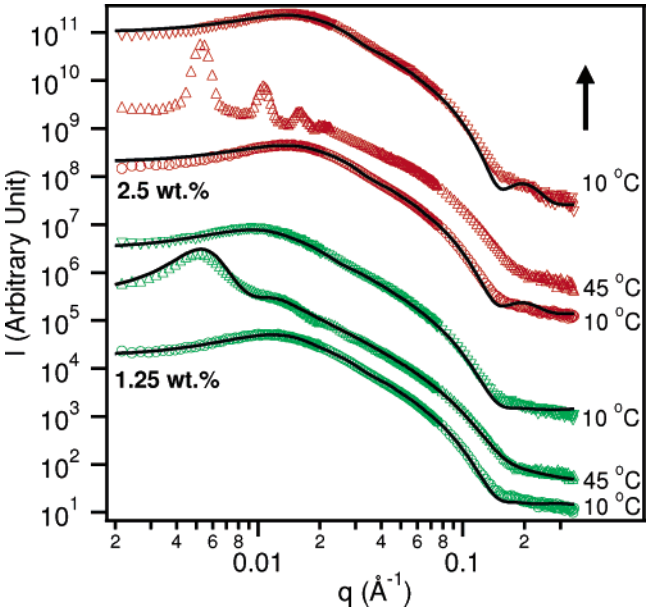

Figure 4. SANS profiles of 2.5 and 1.25 wt % samples, prepared at 10 °C, on heating to 45 °C and cooling back to 10 °C (sequence shown by arrow). The solid lines are fits to the data at 10 and 45 °C using models of bicelles and ULV in combination with the S_HP structure factor, respectively (see Appendix).

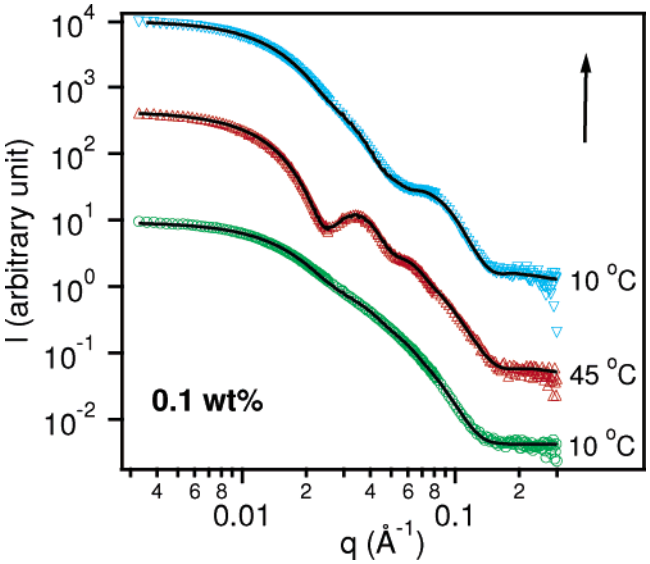

Figure 5. Scattering curves from a 0.1 wt % sample prepared at 10 °C. On heating to 45 °C, bicelles transform into reasonably monodisperse ULV. However, on cooling back to 10 °C, the bicelle morphology is not recovered, but rather the data is best fit by monodisperse oblate ellipsoids (see Figure 1). Heating back to 45 °C gives rise to a scattering curve (not shown) indistinguishable from the one presented here. Fits to the data are depicted by the solid black lines. Temperature sequence is indicated by the arrow.

defects whose edges are lined with DHPC molecules, in which case, one would underestimate the bilayer thickness δ using the simple relation $d = \delta/\phi$.

The higher order Bragg peaks are only prominent for 2.5 wt % $\leq \phi \leq$ 9 wt %. This absence of higher order maxima cannot simply be attributed to instrumental smearing as the width of the Bragg maxima are not instrumental resolution limited ($\Delta q \sim 0.0066$ Å^{-1} at $q = 0.12$ Å^{-1}). It is also not a consequence of a changing morphology as the swelling (d vs ϕ) is nearly one-dimensional, characteristic of lamellar sheets. On the other hand, the form factor for a typical single DMPC bilayer in D_2O decays rapidly in

q.[20] Since the form factor for the same bilayer with increasing level of hydration does not change drastically,[21] then the amplitudes of the quasi Bragg peaks result from sampling that form factor at different values of q. It is therefore not surprising that over the wide range of q measured the first-order amplitude changes and that higher order peaks are not always observable (i.e., 25 wt % sample), except when they appear at lower q (i.e., 2.5 wt % sample), where the magnitude of the form factor is large.

In contrast, the scattering patterns for $\phi \leq 1.25$ wt % do not exhibit sharp Bragg peaks, with the scattering intensity decaying as q^{-2} over an extended q-range (Figure 2). This is consistent with the form factor of locally flat, sheetlike objects such as bilayers making up a ULV. The fact that these scattering curves are devoid of any oscillations indicates that the ULV are highly polydisperse. Fitting the data to a model of noninteracting spherical ULV with a Schulz size distribution (see the Appendix) gives an average radius $\langle R_i \rangle > 1200$ Å with an absolute minimum polydispersity (standard deviation of radius/mean radius) $p \sim 0.25$. It should be noted that values of $p > 0.25$ also fit the data equally well.

It is clear from these observations that the lamellae undergo an unbinding transition at $\phi < 2.5$ wt %. Moreover, the SANS profiles from these lamellae do not exhibit correlated, thermally induced fluctuations as previously seen in dioleoyl phosphatidylserine bilayers.[4,22] Either these fluctuations are absent or the correlation peak occurs at values of q not measured by our experiments. It is also possible that the intermediate state of correlated fluctuating bilayers is not a universal precursor to unbinding. The simple fact that the lamellae cannot remain correlated below a certain ϕ suggests that the lamellar phase may not be thermodynamically stable, in contrast to what was suggested by Leng et al.[12]

It is well established that the low-temperature phase across much of the ϕ range studied is populated by bicelles.[16] Here, we focus on the effect of lowering the temperature on the 1.25 and 2.5 wt % samples, which lie on either side of the unbinding transition (Figure 3). The SANS data do not show any sharp peaks and are well described by the bicelle morphology. The data can be best-fit by a combination of the core−shell−discoidal (CSD) model and the Hayter-Penfold structure factor, $S_{HP}(q)$, (see the Appendix) resulting in a disk core radius, R, of 590 and 220 Å for the 1.25 and 2.5 wt % samples, respectively. Both samples have the same bilayer thickness (42 Å) δ, which for the shell model is the sum of the hydrophobic L and hydrophilic t thicknesses.

On reheating to 45 °C, the lamellae are recovered in all of the samples with $\phi \geq 2.5$ wt %. However, d for the re-formed lamellar phase is smaller presumably because of an increased number of pores/defects populating the lamellae.

Reheating has a very different effect on the 1.25 wt % sample. The scattering pattern shows an oscillatory behavior as a function of q, instead of the monotonic decay initially seen at 45 °C. The data were fit to a ULV model with a $S_{HP}(q)$ structure factor and a Schulz size distribution resulting in an average core radius $\langle R_i \rangle = 312$ Å and bilayer thickness $\delta = 33$ Å, with a polydispersity of $p = 0.14$. Thus, the ULV initally formed by diluting the lamellar phase are recovered upon reheating from the isotropic bicellar phase, indicating ULV thermodynamic stability. However, whereas the ULV were initially large and highly polydisperse, they are now smaller and much less polydisperse.

Weakly scattering Bragg diffraction can, in some cases, be easily confused with scattering from monodisperse ULV; i.e., compare the data in Figure 3 from the two samples reheated to 45 °C. However, it is possible to distinguish the two by carefully fitting the data. A ULV model cannot fit the lamellar SANS data and vice versa.

Low-T Dilution. A second set of samples were prepared by carrying out the dilution process at 10 °C, instead of 45 °C. Again, the dilution occurred in single steps to final concentrations of 2.5, 1.25, 0.5, and 0.1 wt %. Data were collected from these samples first at 10 °C, then on heating to 45 °C, and finally on cooling back to 10 °C. Figure 4 shows the 2.5 and 1.25 wt % data, which, analogous to Figure 3, brackets the boundary of the lamellar−ULV unbinding transition.

At 10 °C, none of the scattering patterns show any sharp features, whereas the data is best described by the CSD bicelle model in combination with $S_{HP}(q)$. The best fit results for $\phi = 0.1$, 1.25, and 2.5 wt % give $R = 141$, 199, and 203 Å, respectively, with $\delta = 40$ Å for all samples. Raising the temperature causes samples with $\phi \geq 2.5$ wt % to transition into the lamellar phase, whereas those with lower ϕ show smoother profiles with oscillations, corresponding to reasonably monodisperse ULV. Bicelles are recovered, at 10 °C for $\phi \geq 0.5$ wt % samples. However, compared to the initial bicelles, the R of these re-formed bicelles are typically larger, i.e., $R = 281$ Å compared 199 Å for the 1.25 wt % sample.

This change in morphology corresponds exactly to the changes as a result of high-T dilution. Clearly, above some critical temperature, T_c, there is a phase boundary between 1.25 and 2.5 wt %. Regardless what path is taken through temperature/concentration phase space, and as long as one terminates at a $T > T_c$, ULV exist below $\phi \sim 2$ wt % and lamellae above. From the exisitence of a phase boundary we infer that the two phases are thermodynamically equilibrium morpholgies.

Low Concentration Morphology. In the above discussion, we argue for the existence of a real phase boundary between the thermodynamically equilibrium phases of ULV and lamellae, based, in part, on the reversibility of the bicelle to ULV or lamellar transition. However, at very low concentrations, we find that the ULV are kinetically trapped, as has been previously suggested.[12]

Interestingly, for the 0.1 and 0.5 wt % samples diluted at 45 °C, lowering the temperature to 10 °C does not result in any changes to the scattering patterns shown in Figure 2, indicating that the large, polydisperse ULV are trapped. This is unlike the higher concentrations, discussed above. Figure 5 shows similar data from the 10 °C dilution 0.1 wt % sample. The sample begins in the bicelle phase, but upon heating forms ULV with an average radius $\langle R_i \rangle = 98$ Å and a polydispersity $p = 0.15$. The small $\langle R_i \rangle / \delta \sim 3$ value shows the presence of high curvature ULV, possibly the result of differences in lipid composition between the inner and outer bilayer leaflets. After the 0.1 wt % sample is re-cooled to 10 °C, SANS data do not show the characteristic scattering pattern for bicelles, but instead, the scattering curve is best fit using monodisperse core−shell oblate ellipsoids with major and minor radii of 180 and 62 Å, respectivly (Figure 5). Reheating the sample to 45 °C yields a scattering curve identical to the one of ULV initially formed from bicelles, indicating that the ULV has conserved its size and mass. Although the shell thickness of the oblate ellipsoid model only approximates

(20) Worcester, D. L.; Franks, N. P. *J. Mol. Biol.* **1976**, *100*, 359.
(21) Katsaras, J.; Stinson, R. H. *Biophys. J.* **1990**, *57*, 649.
(22) Demé, B.; Dubois, M.; Zemb, T. *Langmuir* **2002**, *18*, 1005−1013.

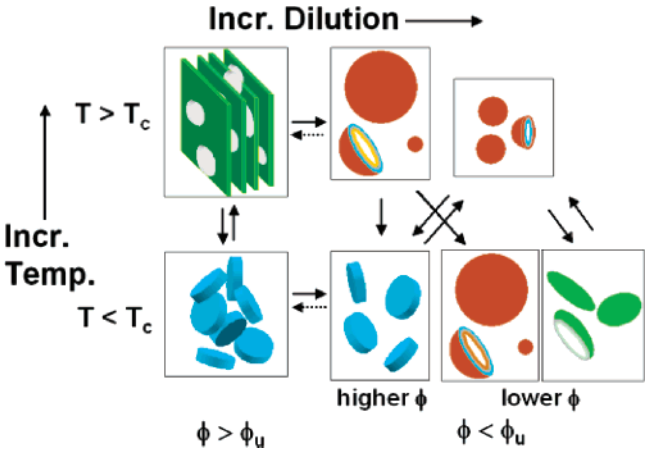

Figure 6. Schematic of the proposed morphological transformations. On diluting below a critical lipid concentration ϕ_u at $T > T_c$, bilayers unbind into a polydisperse ULV dispersion. On cooling below T_c and $\phi_u \geq \phi \geq 1.25$ wt %, polydisperse ULV transform into an isotropic bicellar solution, which on reheating to $T > T_c$, gives rise to monodisperse ULV. For $\phi \leq 0.5$ wt % polydisperse ULV are trapped and cannot transform into bicelles at low T. Monodisperse ULV can also be obtained by diluting the bicellar phase below ϕ_u at $T < T_c$, followed by heating above T_c. In the case of very dilute mixtures, i.e., $\phi \leq 0.1$ wt % and $T < T_c$, bicelles are not recoverable. Instead, oblate ellipsoids are formed. The dashed lines indicate plausible transformations not probed by the present experiments.

the bilayer thickness, the calculated increase in the model shell thickness from 36 Å (ULV) to 45 Å (oblate ellipsoids) is consistent with a bilayer undergoing a transition from the L_α to gel phase. Furthermore, the intensity of the ULV and ellipsoid data at low q converge to similar values, which indicates the size of the aggregates are nearly the same.

This oblate morphology can be understood in terms of the nascent stages of segregation between the gel-phase DMPC and DMPG from L_α DHPC. The long chain lipids form a rigid planar structure, thereby decreasing the curvature energy resulting from the high bilayer bending rigidity κ as T is decreased below T_c. However, since the critical micellar concentration of DHPC is very high, at this low concentration, there may be an insufficient amount of DHPC to stabilize the bicelle's rim. Therefore, the DMPC/DMPG planar bilayers are bridged via the flexible DHPC molecules, forming oblate ellipsoids which we presume are a precursor morphology to bicelles.

These data indicate that, at very low lipid concentrations once ULV are formed, both their morphology and size are trapped. The overall time evolution of the system is unknown, since ULV can be very stable over periods of months.[16] However, we suggest that there is no evolution of *morphology* as the observed structures are believed to be thermodynamically stable, as we have described in detail in a previous section. On the other hand, although ULV are stable, their size may change over extended periods of time.

The various morphological transformations are summarized in Figure 6, and as shown in the figure, ULV size distribution is path dependent. Note that the unbinding of lamellae leads to the formation of large polydisperse ULV, whereas heating from the bicellar phase results in smaller, but reasonably monodisperse ULV. The formation of polydisperse ULV from lamellae is not surprising, since the unbinding of the bilayers does not select any particular length scale. However, the situation is very different when ULV are formed from bicelles. A mechanism similar to that proposed for the lecithin−bile salt system, discussed in the Introduction,[12] is very likely to be taking place here. The reduction in the amount of highly curved edges on forming ULV is most probably the result of varying amounts of DHPC incorporated in the bilayer, as observed previously in a similar "bicellar" system of PC lipids with biphenol substitutions on the acyl chains.[23] In the case of Leng et al.[12] the lamellar to ULV transition is being driven by changing bile salt monomer concentration after dilution, and bicelles are an intermediate morphology as the bile salt leaves the lipid matrix. In this report, bicelles are found to be a highly stable morphology and the bicelle−ULV transition is closely associated the "melting" of the DMPCs hydrocarbon chains and the detergent-like behavior of the DHPC.

Unlike the system presented by Leng et al. where the lamellar phase was presumed to be thermodynamically stable and the ULV was not, we believe that ULV are a thermodynamically stable morphology for the following reasons. First, ULV appear spontaneously, without the input of external energy, whether mechanical, chemical, electrochemical, etc. Second, the ULV phase is determined by the system's total lipid concentration, independent of the method of preparation. Finally, the ULV phase exists in equilibrium with its neighboring single-phase regions in the phase diagram, namely lamellae and micelles (bicelles). At low concentrations, lamellae are no longer a thermodynamically stable morphology since they unbind and form ULV. Those same ULV can be temperature cycled and the ULV morphology is consistently recovered.

The occurrence of differing size ULV, however, raises questions about the thermodynamic stability of their size distribution. Large polydisperse ULV are expected to be stable in systems with either a small bilayer bending rigidity ($\kappa < k_BT$) or near zero spontaneous curvature, whereas smaller, reasonably monodisperse ULV are stable in systems with nonzero spontaneous curvature.[24] In our system, DMPC has large κ and small spontaneous curvature, but when DHPC is added or removed, both parameters may vary significantly. The fact that either polydisperse or monodisperse ULV can be obtained shows that, at best, only one of them can be thermodynamically stable. In the absence of any size-selective energetics, the monodisperse ULV obtained on heating the dilute isotropic phase is unlikely to correspond to the equilibrium distribution. This narrow size distribution changes temporally either by the coalescence of vesicles or by the diffusion of lipid molecules through the solvent. In the present system, both of these processes are expected to be very slow; the first as a result of the charges associated with the ULV, whereas diffusion is limited by the very low concentration ($\sim 10^{-9}$ M) of the long-chain lipids in solution.[1] These distributions are thus effectively frozen over typical experimental time scales. In addition to the kinetics, ULV size evolution can also be retarded by the presumably small differences in the free energy corresponding to different size distributions, which result in very weak thermodynamic forces that drive the system to equilibrium.

4. Concluding Remarks

In conclusion, we observe the spontaneous formation of path-dependent monodisperse and polydisperse phospholipid ULV. Diluting the anionic lamellae results in their complete unbinding, forming highly polydisperse ULV, whereas monodisperse ULV are obtained, for those same

(23) Tan, C.; Fung, B.; Cho, G. *J. Am. Chem. Soc.* **2002**, *124*, 11827.
(24) Jung, H. T.; Coldren, B.; Zasadzinski, J. A.; Iampietro, D. J.; Kaler, E. W. *Proc. Nat. Acad. Sci. U.S.A.* **2001**, *98*, 1353−1357.

samples, on heating from the dilute isotropic bicellar phase. Our SANS data show that for 1.25 wt % ≤ ϕ ≤ 2.5 wt % samples, large, polydisperse ULV transform into bicelles at 10 °C, but for ϕ ≤ 0.5 wt % samples ULV are trapped. For ϕ ≥ 0.5 wt %, bicelles are recovered from small, monodisperse ULV at 10 °C; however, for ϕ = 0.1 wt %, ULV tranform into oblate ellipsoids. These results suggest that the ULV morphology is most likely thermodynamically stable for $T > T_c$ and $\phi < \phi_u$, but that ULV size distribution depends on the equilibrium precursor morphology. The metastability of the ULV size distribution is a reflection of the very slow evolution of the system toward its true equilibrium polydisperse state, probably due to a combination of slow kinetics and weak restoring forces resulting from minute differences in the free energy of the monodisperse and polydisperse ULV.

Acknowledgment. We thank G. Pabst for helpful discussions and the Advanced Foods and Materials Network (Networks of Centres of Excellence, Canada) for financial assistance. This work utilized facilities supported in part by the National Science Foundation under Agreement No. DMR-9986442.

Appendix

(i) Core−Shell Sphere Model. A core shell sphere model is used to model ULV. The spherical shell, i.e., a lipid bilayer, is filled with and surrounded by D_2O. R_o is the outer radius, and R_i is the inner radius of a shell of thickness δ. The Schultz distribution $f(r)$ is used to describe the ULV size distribution, and polydispersity p defined as $\sigma/\langle R_o\rangle$, where σ is the standard deviation and $\langle R_o\rangle$ is the average outer ULV radius. The variance of R_o is given by σ^2. Since the scattering length density (SLD) of the D_2O solvent ($\rho_{solvent}$) is much greater than the SLD of the lipid bilayer's hydrophilic headgroups ($\rho_{hydrophilic}$) and the hydrophobic hydrocarbon chains ($\rho_{hydrophobic}$), we describe the SLD for the shell, ρ_{shell}, as the average of the $\rho_{hydrophilic}$ and $\rho_{hydrophobic}$. The form factor then of a ULV, $P_{ULV}(q)$ can thus be written as follows:

$$P_{ULV}(q) = \frac{1}{V_{ULV}}\int_0^\infty f(r) A_{ULV}{}^2(q, r)\, dr \qquad (1)$$

where V_{ULV} is the total volume of a ULV and

$$A_{ULV}(q, r) = \frac{4\pi(\rho_{shell} - \rho_{solvent})}{q^3} \times [(\sin q\epsilon r - \sin qr) - qr(\epsilon \cos q\epsilon r - \cos qr)]$$

where $\epsilon = \langle R_i\rangle/\langle R_o\rangle$. The Schultz distribution can be written as

$$f(r) = \frac{p^{-2/p^2}}{\langle R_o\rangle\Gamma(1/p^2)}\left(\frac{r}{\langle R_o\rangle}\right)^{(1-p^2)/p^2} \exp\left(-\frac{r}{p^2\langle R_o\rangle}\right)$$

The Gamma function, $\Gamma(1/p^2)$, is used to normalize the integral of the Schultz function and a reasonable value for p is in the range of 0−1. The detailed derivation of eq 1 has been carried out by Hayter.[25]

(25) Hayter, J. B. In *Physics of Amphiphiles*; Degiorgio, V., Corti, M., Eds.; Elsevier: Amsterdam, 1985.

(ii) Core Shell Discoidal Model. Bicelles can adequately be represented by disks with flat, rather than curved edges. The surface of the disks is covered by the phosphorylcholine headroups, whereas the interior inner core is made up of the 14:0 and 6:0 hydrocarbon chains. R represents the hydrophobic core radius, whereas L and t describe the thicknesses of the hydrophobic core and hydrophilic shell, respectively. After orientational averaging, $P_{disk}(q)$, the form factor of a core−shell disk can be expressed in the following manner:

$$P_{disk}(q) = \frac{1}{V_{disk}}\int_0^{\pi/2} A_{disk}{}^2(q,\alpha)\sin\alpha\, d\alpha \qquad (2)$$

where

$$A_{disk}(q,\alpha) = 2(\rho_{hydrophobic} - \rho_{hydrophilic})V_{hydrophobic} \times \frac{\sin\left(q\frac{L}{2}\cos\alpha\right)}{q\frac{L}{2}\cos\alpha}\frac{J_1(qR\sin\alpha)}{qR\sin\alpha} + 2(\rho_{hydrophilic} - \rho_{solvent})V_{disk} \times \frac{\sin\left(q\left[\frac{L}{2}+t\right]\cos\alpha\right)}{q\left[\frac{L}{2}+t\right]\cos\alpha}\frac{J_1(q[R+t]\sin\alpha)}{q[R+t]\sin\alpha}$$

where $J_1(x)$ is the first-order Bessel function and α is the angle between the bilayer normal, **n**, and the scattering vector, **q**. V_i is the volume of lipid species i in the disk. For interacting charged disks, the structure factor has been calculated by Hayter and Penfold.[26]

(iii) Core−Shell Oblate Ellipsoid Model. The oblate ellipsoid model is in many ways similar to the core−shell sphere model. However, this model has a constant shell thickness along the radial direction, which only approximates the bilayer thickness (i.e., thickness in the direction normal to the ellipsoid surface). The form factor for an oblate ellipsoid averaged over all possible orientations of the ellipsoid, $P_{ellipsoid}(q)$, can be expressed as

$$P_{ellipsoid}(q) = \frac{1}{V_{ellipsoid}}\int_0^1 |A_{ellipsoid}(q,\beta)|^2\, d\beta \qquad (3)$$

where the scattering amplitude is given by the difference of two solid ellipsoids, where the core is made of solvent

$$A_{ellipsoid}(q,\beta) = 3(\rho_{core} - \rho_{shell})V_{core}j_1(u_{core})/u_{core} + 3(\rho_{shell} - \rho_{solvent})V_{ellipsoid}j_1(u_{shell})/u_{shell}$$

where j_1 is the first order spherical Bessel function, $j_1(x) = \sin x/x^2 - \cos x/x$, $\beta = \cos\alpha$, the volume of each solid ellipsoid, $V = (4\pi/3)ab^2$, and a, b are the minor and major radii. The orientation for the core ellipsoid is given by $u = q[b^2(1-\beta^2) + a^2\beta^2]^{1/2}$.

The total scattering intensity for noninteracting particles (i.e. disks, ellipses, and ULV) is written as

$$I(q) = \Phi_{lipid}P_{particle}(q)$$

where Φ_{lipid} is the volume fraction of the lipid in solvent. For interacting charged particle, $I(q)$ is multiplied by the structure factor $S_{HP}(q)$ derived by Hayter and Penfold.[26]

LA0508994

(26) Hayter, J. B.; Penfold, J. *Mol. Phys.* **1981**, *42*, 109.